Geochemical behavior of an acid drainage system: the case of the Amarillo River, Famatina (La Rioja, Argentina)

K.L. Lecomte, S.N. Maza, G. Collo, A.M. Sarmiento & P.J. Depetris

Environmental Science and Pollution Research

ISSN 0944-1344

Environ Sci Pollut Res
DOI 10.1007/s11356-016-7940-2

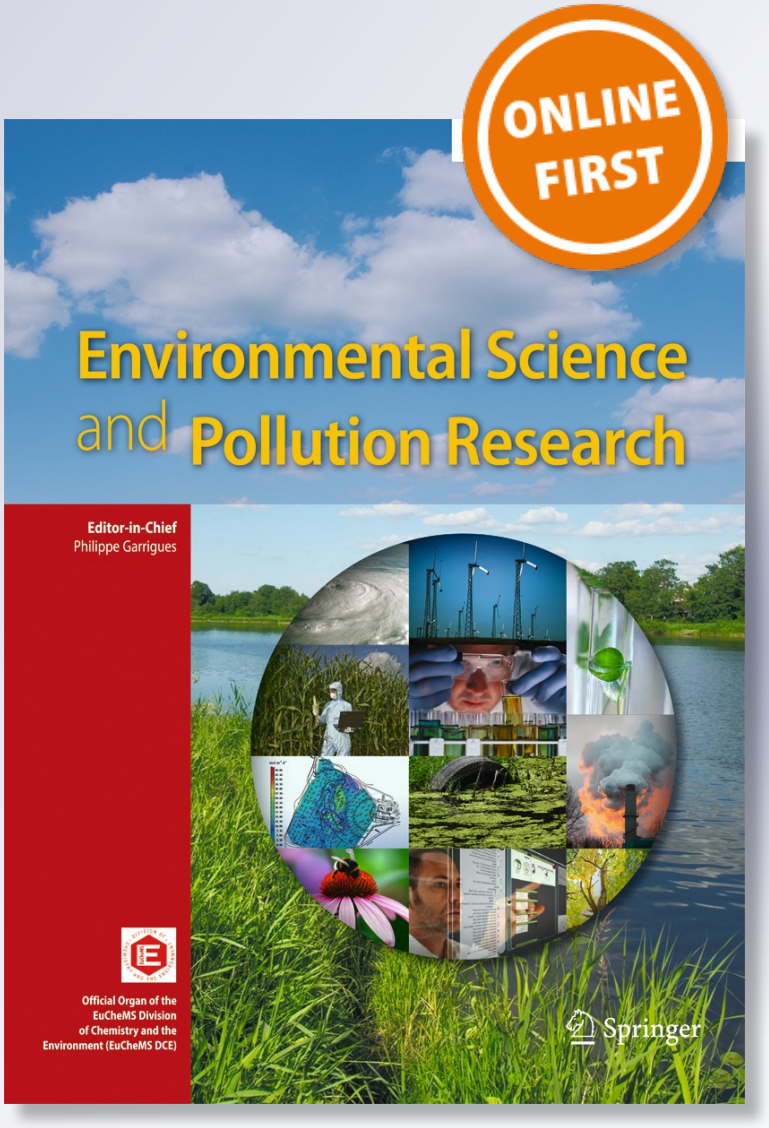

Springer

Your article is protected by copyright and all rights are held exclusively by Springer-Verlag Berlin Heidelberg. This e-offprint is for personal use only and shall not be self-archived in electronic repositories. If you wish to self-archive your article, please use the accepted manuscript version for posting on your own website. You may further deposit the accepted manuscript version in any repository, provided it is only made publicly available 12 months after official publication or later and provided acknowledgement is given to the original source of publication and a link is inserted to the published article on Springer's website. The link must be accompanied by the following text: "The final publication is available at link.springer.com".

Author's personal copy

Environ Sci Pollut Res
DOI 10.1007/s11356-016-7940-2

RESEARCH ARTICLE

Geochemical behavior of an acid drainage system: the case of the Amarillo River, Famatina (La Rioja, Argentina)

K.L. Lecomte[1] · **S.N. Maza**[1] · **G. Collo**[1] · **A.M. Sarmiento**[2] · **P.J. Depetris**[1]

Received: 11 June 2015 / Accepted: 19 October 2016
© Springer-Verlag Berlin Heidelberg 2016

Abstract The Amarillo River (Famatina range, Argentina, ~29° S and ~67° W) is unusual because acid mine drainage (AMD) is superimposed on the previously existing acid rock drainage (ARD) scenario, as a Holocene paleolake sedimentary sequence shows. In a markedly oxidizing environment, its water is currently ferrous and of the sulfate-magnesium type with high electrical conductivity (>10 mS cm^{-1} in uppermost catchments). At the time of sampling, the interaction of the mineralized zone with the remnants of mining labors determined an increase in some elements (e.g., Cu ~3 to ~45 mg L^{-1}; As ~0.2 to ~0.5 mg L^{-1}). Dissolved concentrations were controlled by pH, decreasing significantly by precipitation of neoformed minerals (jarosite and schwertmannite) and subsequent metal sorption (~700 mg kg^{-1} As, 320 mg kg^{-1} Zn). Dilution also played a significant role (i.e., by the mixing with circumneutral waters which reduces the dissolved concentration and also enhances mineral precipitation). Downstream, most metals exhibited a significant attenuation (As 100 %, Fe 100 %, Zn 99 %). PHREEQC-calculated saturation indices (SI) indicated that Fe-bearing minerals, especially schwertmannite, were supersaturated throughout the basin. All positive SI increased through the input of circumneutral water. PHREEQC inverse geochemical models showed throughout the upper and middle basin, that about 1.5 mmol L^{-1} of Fe-bearing minerals were precipitated. The modeling exercise of mixing different waters yielded results with a >99 % of correlation between observed and modeled data.

Keywords Acid rock drainage · Acid mine drainage · Natural attenuation · Efflorescent sulfate salts · Fe-bearing minerals · PHREEQC modeling

Responsible Editor: Philippe Garrigues

Electronic supplementary material The online version of this article (doi:10.1007/s11356-016-7940-2) contains supplementary material, which is available to authorized users.

✉ K.L. Lecomte
karina.lecomte@unc.edu.ar

S.N. Maza
santiagomaz@gmail.com

G. Collo
gildacoll@gmail.com

A.M. Sarmiento
aguasanta.miguel@dgeo.uhu.es

P.J. Depetris
pedro.depetris@gmail.com

[1] Centro de Investigaciones en Ciencias de la Tierra (CICTERRA) CONICET, Universidad Nacional de Córdoba, Av. Vélez Sarsfield 1611, X5016CGA Córdoba, Argentina

[2] Dpto. Geodinámica y Paleontología, Universidad de Huelva, 21071 Huelva, Spain

Introduction

Naturally occurring, extremely acid streams, rivers, and lakes are rare features in nature. Among the mechanisms controlling acidity, "acid rock drainage" (ARD) is conspicuous and refers to acid (pH <5), metal-rich waters that are derived from the weathering of sulfide mineral deposits when exposed to air, water, and microorganisms. There are also natural acid waters which are associated with volcanism or with organic-rich streams in the tropics (e.g., "black waters" as in the Negro River, Amazonia). However, widely known and relatively frequent are the acid waters which an undesirable mining by-products (i.e., acid mine drainage, AMD). Following the

Published online: 28 October 2016

Author's personal copy

growing importance given to water quality and considering AMD, the most important pollution problem determined by global mining, many authors have studied the behavior of dissolved heavy metals in such complex geochemical systems (e.g., Akcil and Koldas 2006; Blowes et al. 2014; Borrego et al. 2005; Cánovas et al. 2012; Delgado et al. 2012; Grande et al. 2010; Hubbard et al. 2009; Jönsson et al. 2005; Lei et al. 2010; Lindsay et al. 2015; Maza 2015; Macías et al. 2012; Nieto et al. 2007; Nordstrom 2009; Olías et al. 2006, 2005, 2004; Pérez-López et al. 2011; 2010; Sarmiento et al. 2011; Younger 1997). The foci of these investigations are generally placed on precipitation of schwetmannite and jarosite and the linked adsorption processes that take place in mining-derived materials, such as tailing impoundment, waste-rock dumps, open pits, and labors. Significant importance is also placed on establishing remediation procedures to ameliorate the negative impact of mining (e.g., Campbell et al., 2015; Caraballo et al. 2011, 2009; Johnson and Hallberg, 2005; Macías et al. 2012).

A pronounced variation in time and space, determined by several physical, chemical, and biological processes, rule the geochemical behavior in acid streams and rivers, whether the processes are natural (ARD) or human-made (AMD). The formation of acid water will depend on the balance between the potential acidity of the outcropping rocks (amount and kind of sulfurs) and the probable neutralization of the surrounding deposit. In this way, there are a group of geochemical processes which can be summarized as follows: the first stage of weathering is mineral oxidation by O_2 (Eq. 1), where mainly pyrite but also pyrrhotite, marcasite, chalcopyrite, sphalerite-galena, and arsenopyrite are the minerals that generate most acidity. The overall redox reaction is

$$FeS_2 + 7/2\ O_2 + H_2O \rightarrow Fe^{2+} + 2SO_4^{2-} + 2H^+ \quad (1)$$

where ferrous iron (or Fe(II)), sulfate, and acidity are released to the solution by pyrite. Then, Fe^{+2} is oxidized to Fe^{+3} (Eq. 2) and, later, it is hydrolyzed and precipitated as a solid phase (i.e., $Fe(OH)_3$ and other chemical species) releasing $3H^+$ (Eq. 3). The latter reaction is catalyzed by microorganisms (e.g., acidic bacteria as *Thiobacillus ferrooxidans*; Kawano and Tomita, 2001), increasing reaction kinetics by several orders of magnitude:

$$Fe^{2+} + 1/4\ O_2 + H^+ \rightarrow Fe^{3+} + 1/2\ H_2O \quad (2)$$

$$Fe^{3+} + 3\ H_2O \rightarrow Fe(OH)_{3(s)} + 3H^+ \quad (3)$$

Iron hydrolysis is an exothermic reaction and is the main source of acidity that generates ideal conditions for the bacterial growth (pH in the range of 1.5–4 and temperature in the 25–45 °C range; Kozubal et al. 2012; Urbieta et al. 2014). Combining reactions 2, 3, and 4, the following overall reaction is reached:

$$FeS_2 + 15/4O_2 + 7/2H_2O \rightarrow Fe(OH)_3 + 2SO_4^{2-} + 4H^+ (4)$$

Fe^{+3} is also another important oxidizing agent which generates more acidity than does O_2, as shown in Eq. 5:

$$FeS_2 + 14\ Fe^{3+} + 8H_2O \rightarrow 15\ Fe^{2+} + 2SO_4^{2-} + 16H^+ \quad (5)$$

These are the main processes that define both mechanisms, ARD and AMD.

The results of the evolution of these chemical systems, once the neutralizing capacity of the environment has been exceeded, are waters with large amounts of dissolved sulfate, Fe, and other metals, such as As, Cd, Co, Cu, Pb, Zn, etc. The high concentration of total dissolved solids (TDS) is determined by the increased mineral dissolution rate that is normally associated with distinctly acid environments (Nordstrom 2011; Nordstrom and Campbell 2014; Nordstrom et al. 2015). The formation of new minerals, with its consequent coprecipitation and adsorption processes and the mixing with more diluted water tend to decrease the concentration of dissolved elements in the system. As was pointed out by several authors, high dissolved metal concentrations produced by AMD could be naturally attenuated by one or more such mechanisms (e.g., Acero et al. 2006; 2007; Asta et al. 2009; 2010a; 2010b; Bigham et al. 1996; Bowell and Bruce 1995; Brown and Glynn 2003; Cánovas et al. 2008; Chen and Jiang 2012, Cidu et al. 1997; Fernández-Remolar et al. 2006; Fukushi et al. 2003; Gandy et al. 2007; Maza 2015; Meck et al. 2011; Sanchez-España et al. 2005a, 2005b; Sarmiento et al. 2009).

There are some rivers affected by acid drainage in Argentina's Northwest (Famatina range, Province of La Rioja). An interesting example is the Amarillo River, which maintains an acid pH all along the water course. Amarillo River headwaters run through Cu (Mo-Au) porphyry deposits and high-sulfidation veins of Cu–Au (Ag–As–Sb–Te), along with the associated alteration zones, which constitute the Nevado de Famatina Mining District. During the first quarter of the last century, La Mejicana mine was operative, and mineral debris was transported downstream, reaching the town of Chilecito (La Rioja, Argentina). Minimal mining waste material was left at the mine site, although there are a few galleries still visible. Therefore, the scope of this investigation was to analyze geochemical processes in an environment with both, natural and anthropogenic water acidification mechanisms. Attenuation processes were also identified and modeled focusing, as well, on the assessment of such attenuation system in a hyperarid drainage network. These objectives were pursued in the certainty that these studies would be valuable at the time of starting new mining activities. Exposing natural geochemical attenuation is as important as describing geochemical processes that generate high amounts of dissolved metals.

Author's personal copy

Site description

The Amarillo River headwaters are exposed to intensive weathering through aggressive geochemical processes. In this region, the critical zone (Brantley et al. 2007, Stumm and Sulzberger 1992)—where chemical, biological, physical, and geological processes operate together—is complex and dynamic. For example, the oxidation zone can be scarcely superficial or can reach a depth of ~190 m.

This fluvial system in the Famatina Belt drains headwaters through an important halo of high-sulfidation epithermal deposits (Au–Cu–Ag–As–Sb–Te) (Losada-Calderon and McPhail 1994; Pudack et al. 2009), which had been influenced by mining since the nineteenth century until 1925 (La Mexicana Mine). Underground workings were developed, especially on vein galleries connected by shafts and chimneys.

The Famatina Belt is located between 27° and 31° S and is part of the current broken foreland of the Sierras Pampeanas of Argentina (Fig. 1). The Amarillo River basin mainly involves low-grade Cambro-Ordovician fine-grained sedimentary units from the Negro Peinado and Achavil formations and the mineralized porphyry copper area, associated with a hydrothermal-hypabyssal polymetallic process that began with the intrusion of the Mogote Formation (5.0 ± 0.3 Ma, dacitic and rhyodacitic porphyries, Losada-Calderon and McPhail 1994). It must be highlighted that high-sulfidation epithermal deposits and disseminated porphyries also outcrop in the region as several smaller districts. The most important hypogenic mineral is pyrite, accompanied by molybdenite, calcopyrite, enargite, and bornite. Within the hydrothermal alteration, the phyllic alteration consisting of sericite-pyrite-quartz has the largest areal distribution, affecting all lithologies. In Fig. 1c, there is a profile of the area (A-A') showing El Mogote porphyries, quartz-sericite-pyrite veins, and the alteration halo.

The area has a continental, high-mountain (top height ~6000 m a.s.l.) hyperarid climate, with mean annual rainfall of about 200 mm. Intense rainfall occur in summer usually causing torrential floods. The Amarillo River has a drainage basin of 155 km^2, with mean discharges of ~2000 L s^{-1} during the austral summer and ~700 L s^{-1} in the dry season (i.e., wintertime) in the lower basin (Alto Carrizal, Fig. 1), reaching its minimum discharge during October and November (Fernández-Turiel et al. 1995). This high-mountain river is typified by turbulent reddish-yellowish waters transporting a significant load in solution, characterized by a dominance of iron and clay-size phases (Maza 2010, Maza 2015). Achavil and Del Marco rivers are tributaries of the Amarillo River, and downstream, they form the ephemeral Famatina River, which discharges its waters into the alluvial fans of the endorheic system of Paimán-Velasco.

Less than 20 km downstream from the upper catchments, there is a paleolake (Figs.1 and 3) which provides the necessary and sufficient evidence to sustain the acidic nature of the system for the last 3500 years (Maza, et al. 2014; Maza 2015). The accumulated sediments form a 44-m thick lacustrine banded sequence, with varve-like silt-clayed ochres, sandstones, conglomerates, and breccias, associated with the damming of the Amarillo River. The significant amount of unusually well-preserved ochreous sediments (jarosite and goethite, Maza et al. 2014) in this unit was linked to the contribution of a paleo acid drainage associated with polymetallic deposits from the Nevado de Famatina Mining District. The levels are characterized by high concentrations of Fe_2O_3, Cu, Zn, As, Co, and Mo and low concentrations of SiO_2, Al_2O_3, K_2O, MgO, CaO, and Na_2O. The evolution of the paleolake levels was inferred from the analysis of sediments and waters of the present-day Amarillo River catchment. The formation of the iron ochre layers is clearly connected with the pH of river water and with the Fe and SO_4^{2-} concentrations (Maza et al. 2014).

Material and methods

Water samples

In order to assess the hydrogeochemistry characteristics of the system, one sampling was performed during the dry season. Figure 2 shows the mean rainfall and the estimated flow rates at the town of Famatina. Precipitation data (period 1913–1990) was obtained from Torres et al. (2007), whereas discharges were measured during the years 2010–2015 with a Pasco flow meter. Although the discharge increase after humid period is evident, this type of mountainous rivers commonly suffer sudden and violent flow increase when precipitation starts. Such flow peak only lasts a few hours, significantly modifying the hydrological and hydrochemical regimes. Cánovas et al. (2012) explained hydrochemical changes (e.g., releases, remobilization, and mineral precipitation) after a rainfall event in an AMD. Taking into account that the intense rainfall not only dilutes the system but also alters the chemical characteristics, the dry season was selected for sampling because the highest and relatively constant concentrations are reached.

Amarillo River surface water samples were collected in November 2008, from the uppermost catchments downstream to the town of Famatina and from two lateral tributaries that supply their discharges to the main channel (Fig. 3). Table 1 shows the location of sampling sites. Sample RA1 was the uppermost sample, influenced neither by La Mejicana mine nor by the Mogote dacitic porphyry (i.e., the mineralized zone in the profile of Fig. 1c). Downstream, water infiltrates and then outcrops after passing through the mineralized zone,

Author's personal copy

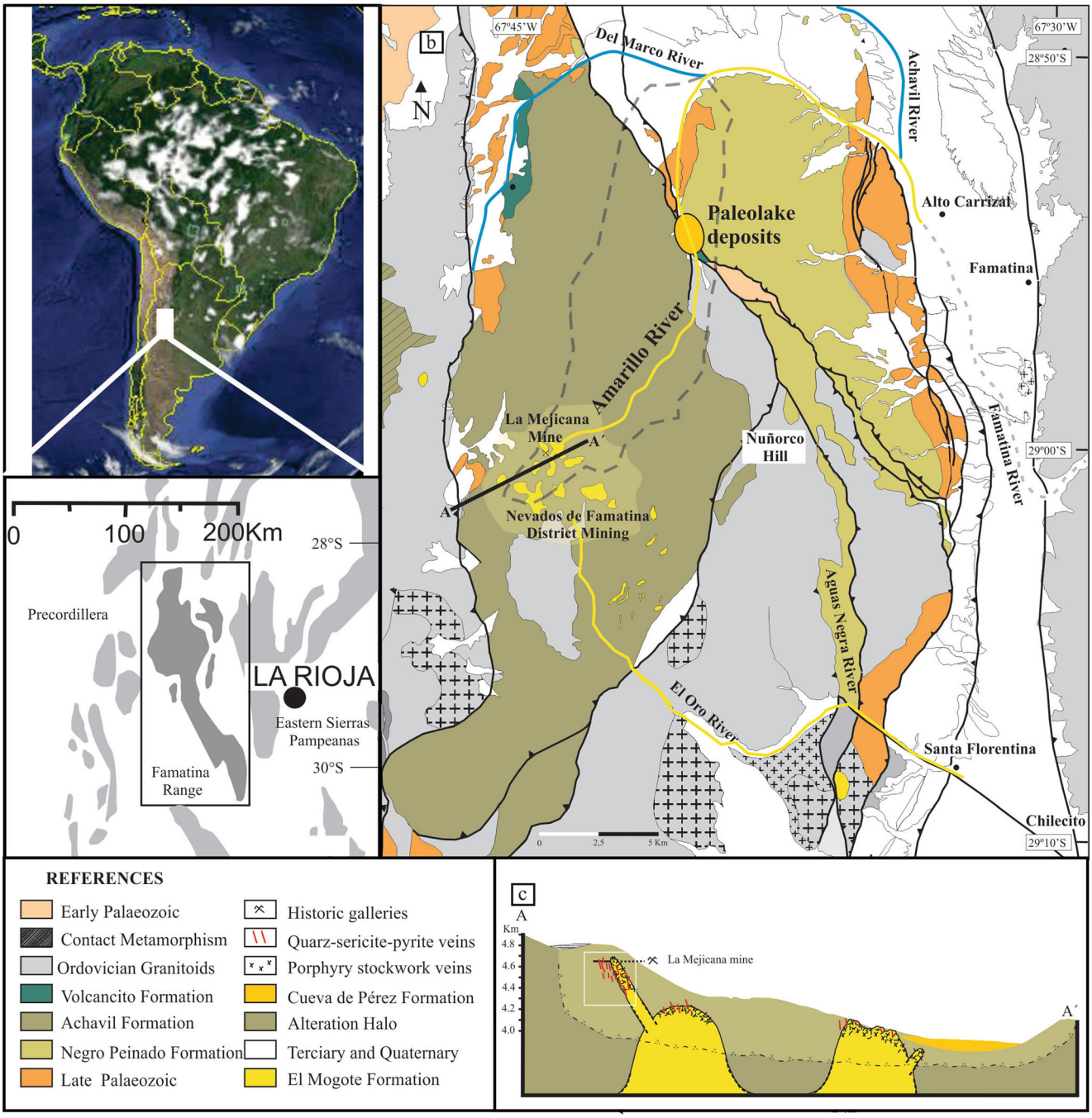

Fig. 1 Map of the study area and sketchy geology: **a** Famatina Range, **b** mineralized zone, lithology, and Amarillo River; **c** schematic profile of the mineralized area modified from Pudack et al. (2009)

generating a swampy area where sample RA2 was collected (Fig. 3). Downstream of this point, the river becomes clearly affected by the remnants of ancient mining.

All samples, from RA3 down to RA12 were collected in the main channel, the last one after joining del Marco and Achavil rivers. Samples RL5 and RL7 were collected in tributary creeks, and RAC5 was collected a few meters below the confluence of the Amarillo River (RA5) with a tributary brook (RL5, Fig. 3).

Water temperature, pH, redox potential, electrical conductivity, and alkalinity (in tributaries) were measured in situ. Redox potential (Eh) was corrected with the usual hydrogen electrode procedure, following Eq. 6 (Nordstrom and Wilde 1998), where T is temperature in °C:

$$Eh = Ec + 223.8 - 1.02\,T \quad (6)$$

Alkalinity was measured as $CaCO_3$, using a 0.1600 N H_2SO_4 solution until pH = 4.5. End point titration was reached

Author's personal copy

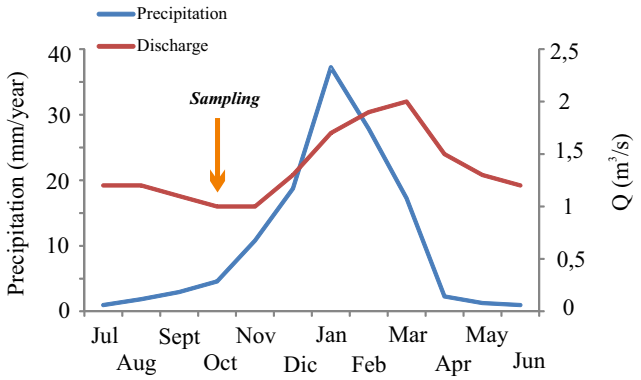

Fig. 2 Mean rainfall and estimated flow rates at Famatina town. Precipitation data (period 1913–1990) was obtained from Torres et al. (2007), whereas discharges were measured during the years 2010–2015 with a flow meter Pasco

in unfiltered water. For subsequent determinations, samples were vacuum-filtered in the field with 0.22-μm pore-size cellulose filters (HA-type, Millipore Corp.). Samples were also acidified (pH <2) with concentrated, redistilled, and ultrapure HNO_3 (Sigma-Aldrich) for the analytical determination of major, minor, and trace elements by inductively coupled plasma-mass spectrometry (ICP-MS) in the more diluted waters, such as RL5 and RL7, or by ICP-OES for the remaining samples (Activation Laboratories Ltd., Ancaster, Ontario, Canada). Detection limits were different in both cases and are reported in the corresponding tables. The results for major, minor, and trace elements were validated using National Institute of Standards and Technology (NIST) 1640 and Riverine Water Reference Materials for Trace Metals certified by the National Research Council of Canada (SRLS-4).

Sediment samples

From every water sampling point, stream bed sediments were also collected and, in some cases (where discernible), crusts and soluble efflorescent sulfate salts. The mineralogical composition of sediments and efflorescent salts was determined by X-ray diffraction (XRD) with a Panalytical X'Pert PRO diffractometer. Conditions were 40 kV and 40 mA, at a speed of 1°/min, between 3° and 60° 2θ, in as much as the main reflections of iron oxide/hydroxide/sulfate/hydrosulfide are found within this range. For clay-size mineral identification, the samples were scanned between 3° and 40° 2θ. Samples were dried at room temperature, and ~10 g of each total sample was ground in an agate mortar until reaching adequate fine grain size (~325 mesh).

Major and trace element concentrations of efflorescent salts and crusts were determined by X-ray fluorescence in some samples, using Bruker S4 Explorer equipment. The chemical composition of bed sediments was determined by ICP (major

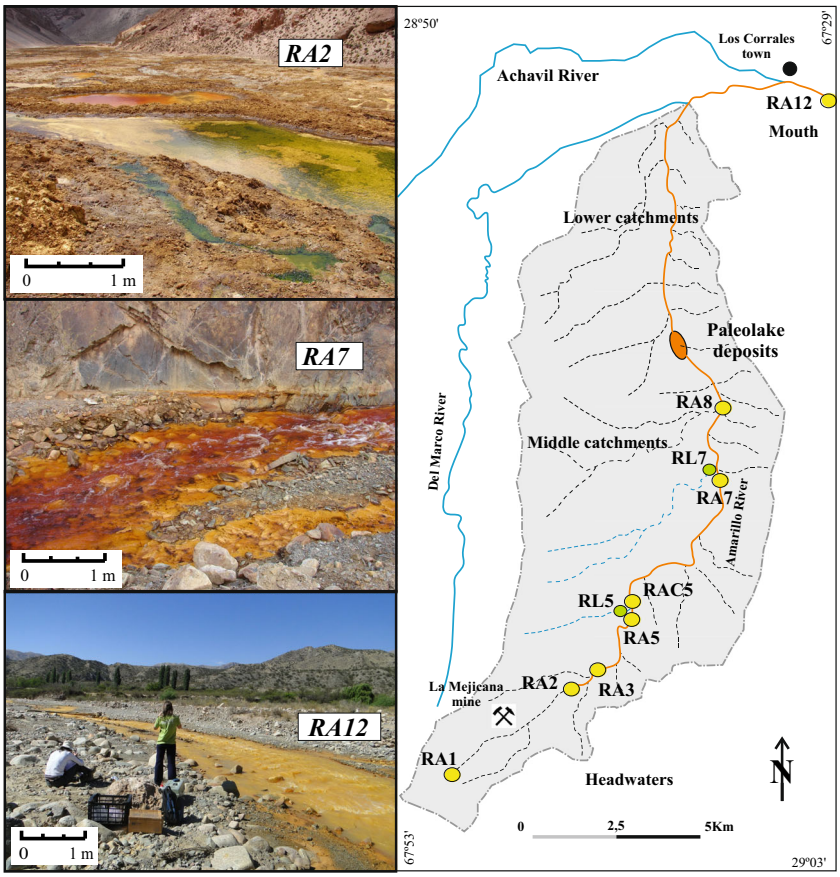

Fig. 3 Amarillo River drainage basin, indicating sampling points. Photographs correspond to representative sampling sites Note changing water color

Author's personal copy

Table 1 Location of sampling points

Sampling gage	Kind of sample	Latitude (S)	Longitude (W)	Height (m a.s.l.)	Downstream distance (km)
RA1	Frozen spring	29° 01′ 00.9″	67° 46′ 59.3″	4600	0.00
RA2	Upwelling water	28° 59′ 51.6 ″	67° 44′ 21.4″	3869	4.89
RA3	Amarillo River	28° 59′ 48.2″	67° 43′ 57.6″	3853	5.54
RA5	Amarillo River	28° 58′ 34.6″	67° 42′ 54.3″	3454	8.83
RL5	Lateral stream	28° 58′ 35.0″	67° 42′ 54.6″	3453	–
RAC5	Amarillo River	28° 58′ 34.5″	67° 42′ 54.8″	3452	8.84
RA7	Amarillo River	28° 56′ 28.9″	67° 40′ 53.6″	2972	15.19
RL7	Lateral stream	28° 56′ 28.6″	67° 40′ 53.8″	2971	–
RA8	Amarillo River	28° 55′ 36.4″	67° 40′ 34.1″	2848	17.09
RA12	Amarillo River	28° 51′ 03.9″	67° 36′ 51.5″	1953	34.37

elements by fusion-inductively coupled plasma—FUS-ICP—while trace elements by total digestion-inductively coupled plasma—TD-ICP—and Instrumental Neutron Activation Analysis—INAA). The laboratory sample preparation consisted in the separation of 15 g of material using a plastic spatula, and the subsequent comminution was performed with an agate mortar.

Geochemical modeling

The PHREEQC 2.18 geochemical code (Parkhurst and Apello 1999) was used to estimate the speciation, activities, and solubility calculation of metals. WATEQ4F (Ball and Nordstrom 1991) was the thermodynamic database used and it was expanded with data from Acero et al. (2007) to account for the solubility of some minerals. Schwertmannite has been proposed as a metastable iron mineral-controlling iron precipitation, and concomitantly water chemistry, over a wide range of acid pH (Bigham et al. 1994; 1996; Bigham and Nordstrom, 2000; Majzlan et al., 2004). Three quite different log Ksp values for schwertmannite are commonly accepted and used to model schwertmannite solubility (Kawano and Tomita, 2001; Yu et al., 1999 and Bigham et al., 1996). However, Caraballo et al. (2013) suggested that schwertmannite's log K_{sp} is related to its chemical composition in the understanding that it is a polyphasic nanomineral. Thus, they propose using a wide log K_{sp} range to model its solubility in nature.

In order to determine in this work schwertmannite's solubility product, the x value was calculated for each sampling point, following Caraballo et al.'s (2013) approach:

$$\mathrm{Log}\left(a^2{}_{\mathrm{H}} + a_{\mathrm{SO4}}{}^{2-}\right) = -11.48 + 2.094x \quad (7)$$

Subsequently, the schwertmannite formula was calculated as

$$Fe_8O_8(OH)_{8-2x}(SO_4)_x \quad (8)$$

Finally, log K_{sp} was calculated following Eq. 9:

$$\mathrm{Log}\ K_{sp} = 8\log a_{\mathrm{Fe+3}} + x\log a_{\mathrm{SO4}}{}^{2-} + (24{-}2x)\mathrm{pH} \quad (9)$$

Table 2 lists x and K_{sp} values for each sampling point. When pH > 4, x exhibits a negative value, as in samples RAL5, RAL7, and RA12, whereas in samples with pH < 4, x varies from 1.22 to 2.23, close to those calculated by Caraballo et al. (2013) (i.e., from 0.5 to 2). The K_{sp} obtained for the Amarillo River agree with the range proposed by those authors (from 5.8 to 39.5).

However, as the systems' behavior is highly dynamic, and each river stretch presents differing K_{sp} values which not only change over space but also in time, it was decided to use Bigham et al.'s (1996) database to run the models in as much their K_{sp} (18.0 ± 2.5) was close to the solubility products calculated for the Amarillo River (Table 2).

This geochemical speciation model is capable of computing equilibrium ion activities among dissolved and adsorbed species and the solid phase in equilibrium. The model uses the interaction of metals with major anions as a function of temperature, *pe* (calculated from redox potential), pH, and ionic strength. Geochemical modeling was accomplished by means

Table 2 Calculated x and Ksp values for each sampling point, following Caraballo et al. (2013) equations

	pH	x	Log K_{sp}
RA1	3.26	2.23	16.78
RA2	3	1.61	26.75
RA3	2.93	1.68	25.02
RA5	2.93	1.65	24.23
RL5	*6.4*	*−2.39*	–
RAC5	3.4	1.22	32.11
RA7	3.2	1.38	25.99
RL7	*7.91*	*−3.79*	–
RA8	3.33	1.22	28.79
RA12	*4.45*	*−0.03*	–

Author's personal copy

of PHREEQC, including inverse modeling and mixing of waters.

Inverse modeling begins with a known initial solution and available mineral phases and attempts to quantify the processes that lead to the final solution chemistry (e.g., Lecomte et al., 2005). To do this, the model reconstructs all possible combinations of dissolution and/or precipitation reactions that explain the chemical changes observed between these two solutions and the mineral phases (Parkhurst and Apello 1999). Mixing modeling gives the final chemistry by mixing solution fractions.

The PHREEQC geochemical code is often used in acid environments mainly to calculate speciation-solubility indexes (e.g., Acero et al. 2006; Asta et al. 2010a; Bigham et al. 1996; Caraballo et al. 2013, Kawano and Tomita 2001). In this work, PHREEQC was also used to simulate (a) weathering/precipitation processes through inverse modeling and (b) the mixing of the Amarillo River and a tributary creek. In our case, it was used when a tributary stream reached Amarillo River main channel, and then the model's output was compared with the observed chemistry.

Results and discussion

Geochemistry of dissolved phases

Table 3 shows the main physicochemical characteristics and the concentration of major elements measured in the samples. The unfiltered water color varied from red (uppermost catchments), orange (middle basin), to yellow (in the lowermost reaches) due to iron speciation. River water remained acid all along the main course; pH ranged from 2.93 to 4.43. It is noticeable that the pH decreased after crossing the abandoned mine and the mineralized zone. Downstream, the buffering effect of iron kept pH constant at ~3 almost throughout the entire drainage basin (the exception is in the lowermost point RA12, where pH reaches 4.5). On the other hand, tributary creeks showed a mean pH of ~7. Water temperature in RA1 was ~5 °C and increased up to >15 °C in the lower basin during the spring afternoon.

During the dry period sampling, the absence of suspended sediments (particle grain-size >0.22 μm) was conspicuous, at least down to RA12. However, electrical conductivity varied from more than 10 mS cm^{-1} in the uppermost catchments, decreasing downstream to <1 mS cm^{-1}, with a mean gradient of ~0.3 mS cm^{-1} km^{-1}. This process adds to the evidence of the occurrence of mechanisms that significantly reduced the concentration of dissolved elements.

According to Piper classification (1944), these acid waters were of the magnesium sulfate type throughout the basin. The uppermost catchments represented a "magnesium end member" in the Piper diagram, connected with cupper porphyry's

Table 3 Main physicochemical characteristics of water samples

ICP-OES detection limit	Distance (km)	pH	Eh	Temp (°C)	Electrical conductivity (mS cm^{-1})	HCO_3 (mg L^{-1})	SO_4^{-2}	Ca	Na	K	Mg	Si	Al	Fe	Mn	P
							0.3	*0.1*	*0.1*	*0.1*	*0.1*	*0.1*	*0.1*	*0.01*	*0.01*	*0.02*
RA1	0	3.26	641	4.9	10.50	0	9884	291	162	0.5	1580	17.4	166	153	580	0.5
RA2	4.9	3	667	9.6	5.78	0	5241	41.6	93.1	50.0	94.2	39.7	542	1220	65.2	3.3
RA3	5.5	2.93	674	9.6	5.56	0	5301	46.7	80.4	33.5	91.3	45.0	568	1110	52.6	3.2
RA5	8.8	2.93	674	9.3	4.15	0	4013	38.5	62.4	13.6	73.9	36.7	419	761	42.3	2.1
RL5	8.8	6.4	320	8.6	0.54	137.3	30.09	20.0	6.2	1.6	20.0	5.8	0.12	0.11	4.40	n.d.
RAC5	8.8	3.4	626	8.2	2.97	0	3265	37.0	41.5	11.5	66.1	29.4	323	549	34.8	1.6
RA7	15.2	3.2	647	15.1	2.62	0	2701	38.8	35.1	9.6	59.4	28.1	268	297	28.9	1.1
RL7	15.2	7.91	165	13.1	0.24	103.7	34.88	20.0	7.3	0.8	14.4	5.0	0.01	0.01	0.002	n.d.
RA8	17.1	3.33	634	5.7	2.09	0	1845	33.2	19.6	6.9	44.0	21.2	185	196	19.6	0.7
RA12	34.4	4.45	519	15.5	0.95	0	494.2	59.0	62.2	6.5	32.7	11.4	30.7	0.12	3.77	0.2
Tinto River (Cánovas et al. 2007)	–	2.82	723	19.6	2.49	–	1449	76.6	39.7	4.0	77.4	75.6	78.7	151	8.0	n.d.

Mean Tinto River chemical compositions have been added for comparison (Cánovas et al. 2007)

Author's personal copy

mineralogy and a chlorite-epidote association discernible in the propylitic alteration zone.

Thus, an acid drainage located upstream of mining that corresponds to an ARD can be identified in the uppermost catchments. On the other hand, downstream from La Mexicana mine, drainage sources present both influences: natural and from the abandoned galleries (AMD).

A comparison with the dissolved chemistry of other similar system (e.g., Tinto River, Cánovas et al., 2007, Tables 3 and 4 show that in the uppermost catchments, there are many components which reach higher concentrations in the Amarillo River (e.g., Al, Cd, Cr, Cu, Fe, K, Mg, Mn, Na, Ni, $(SO_4)^{2-}$, and Zn). However, the sequence of decreasing relative abundance is similar to Tinto River data. The dissolved concentrations >1 mg L^{-1} in Amarillo River are as follows: $(SO_4)^{2-}$ >Fe >Al >Mg >Na >Ca >Mn >Zn >Si >Cu >K >P; outstanding differences are the concentrations of Si and P, which is <1 mg L^{-1}, in Tinto River.

Comparing Amarillo River's dissolved concentrations with the outcropping low-grade metamorphic rocks (i.e., Achavil Fm, Collo, 2006), it is interesting to point out the high concentrations reached by some elements in water. There are some elements that have higher concentrations in the river than in the rocks, such as S, Zn, and Cu. High dissolved elemental concentrations are characteristic of this type of system, where very acidic pH promotes the supply of elements to the solution. This is also evident when compared with lateral tributaries in the same region and also with a stream in a similar Andean climate (e.g., hyper-arid, San Juan, Argentina, Lecomte et al., 2008a). The difference between them, reaches almost six orders of magnitude in some elements such as Al, Mn, Cu, Co, and Cd.

Downstream, most elements decrease concentration, including sulfate. Sulfate ion is a good indicator of AMD contamination because it is a non-reactive compound which is found in large concentrations in acidic leachates and in low concentrations in the AMD-unaffected rivers (e.g., Sarmiento et al. 2009). In acidic waters, the importance of natural chemical processes in removing sulfates from the water is insignificant when compared to dilution processes.

In the main channel, elements were incorporated into efflorescent salts or in the precipitated minerals not only as part of mineral structures but also by the affinity of metals for sorption or coprecipitation with Fe or Al oxi/hydroxy/sulfates. For example, Acero et al. (2006), Asta et al. (2010a), Nagorski and Moore (1999), and Sanchez-España et al. (2005a, 2005b) demonstrated that As and other elements adsorb onto schwertmannite and jarosite. Nevertheless, the concentration decrease of elements clearly showed that the effect of neutralization by dilution with additional water inputs is another important attenuation process. It is clear that the geochemical dynamics of an acid drainage is completely different from a circumneutral hydrological system. Lecomte

Table 4 Dissolved element concentrations in the study area

ICP-OES Detection limit	U	As	Be	Cd	Ce	Co	Cr	Cu	Mo	Ni	Pb	Sb	Se	Sr	Te	Tl	V	W	Y	Zn
	μg L^{-1}																			
	50	*30*	*2*	*2*	*30*	*2*	*20*	*2*	*5*	*5*	*10*	*10*	*20*	*10*	*10*	*10*	*10*	*10*	*10*	*5*
RA1	120	160	32	884	410	990	150	3080	24	533	190	<10	300	640	120	1260	<10	8070	590	421,000
RA2	<50	510	12	914	60	834	260	39,900	163	1040	600	130	110	140	90	180	230	840	40	50,900
RA3	180	300	12	712	60	873	280	46,200	94	1120	670	130	100	110	90	160	240	800	50	43,900
RA5	100	120	10	515	50	630	200	32,500	26	833	500	60	70	70	60	130	130	550	40	31,800
RL5	0.04	0.26	<0.1	1.08	0.288	0.735	<0.5	4.6	0.6	15.6	0.2	<0.1	0.2	71	<0.1	<0.001	0.1	<0.002	0.389	250
RAC5	<50	30	7	386	40	468	160	24,800	12	652	380	40	50	70	40	100	60	430	30	26,100
RA7	<50	60	7	324	40	404	130	20,600	<5	558	340	<10	40	80	30	80	<10	360	30	21,300
RL7	0.13	1.85	<0.1	0.03	<0.001	0.012	< 0.5	0.9	2.2	<0.3	0.2	<0.1	0.3	45	<0.1	<0.001	0.2	< 0.002	<0.003	6.1
RA8	<50	50	4	219	<30	276	90	13,600	<5	382	230	<10	20	70	20	60	<10	250	20	14,200
RA12	<50	<30	<2	38	<30	53	<20	2530	<5	79	50	<10	<20	210	20	10	<10	50	20	2840
Mean Tinto River (Cánovas et al. 2007)	n.d.	160	3	118	n.d.	564	16	18,900	n.d.	170	130	n.d.	n.d.	280	n.d.	n.d	n.d.	n.d	n.d.	26,000

Mean Tinto River chemical compositions have been added for comparison (Cánovas et al. 2007)

n.d. not determined

Author's personal copy

et al. (2008b) studied several mountainous rivers and concluded that the chemical signals were fairly similar: the highest concentrations were reached by incompatible (large ion lithophile elements) due to the release of relatively more soluble elements, whereas those with depleted normalized concentrations were the compatible (high field strength elements) due to the resistance to weathering of host minerals. However, major cations (Mg, Ca, Na, and K) showed the "normal" chemical behavior, which is governed by solubility, i.e., although they were more concentrated, every sample followed the same pattern shown by Lecomte et al. (2008b).

Based upon the dacitic porphyry and high-sulfidation veins presented in Fig. 1c, the scheme in Fig. 4a shows the inferred position of mineral alterations in the uppermost catchments. The scheme of Pudack et al. (2009) was modified by using field mineralization observations, a conceptual model (Giggenbach, 1997; Lowell and Guilbert, 1970), and dissolved geochemistry. Chemical results showed that there were two groups of elements that presented high and significant correlation coefficients ($r > 0.85$, $p < 0.05$, not shown) within each group, which suggest different dissolved load sources. In one of them, there were elements that resulted from the weathering of propylitic alteration zone hosted by metasedimentary rocks (Fm Achavil), associated to porphyry area of the porphyry copper system. This zone presents quartz, plagioclase, chlorite, illite/mica, and kaolinite which are locally crosscut by quart-sericite-pyrite veins that contain at most minor amounts of bornite, idaite, chalcocite, chalcopyrite, covellite, sulfosalts, and sphalerite (Pudack et al., 2009; Wunderlin et al., 2014). The water chemistry shows maximum concentrations in the uppermost sampling point and a decreasing trend downstream throughout the entire basin (e.g., Group 1, Zn, Mg, S, Mn, Ce, Y, Se, W, Te, Tl). In the other group, there were elements which were released by the leaching of the mineralized central zone of the porphyry copper system and closely associated high-sulfidation epithermal veins. The vein material consists of famatinite, enargite, pyrite, and alunite in variable proportions, with minor quartz, kaolinite, dickite, pyrophyllite, tennantite, tetrahedrite, sphalerite, gold, tellurides, covellite, and chalcopyrite (Pudack et al., 2009; Wunderlin et al., 2014), which were also influenced by mining labors (e.g., Group 2, V, Sb, Al, Si, Fe, P, Cr, Ni, Cu, Pb, As, Mo).

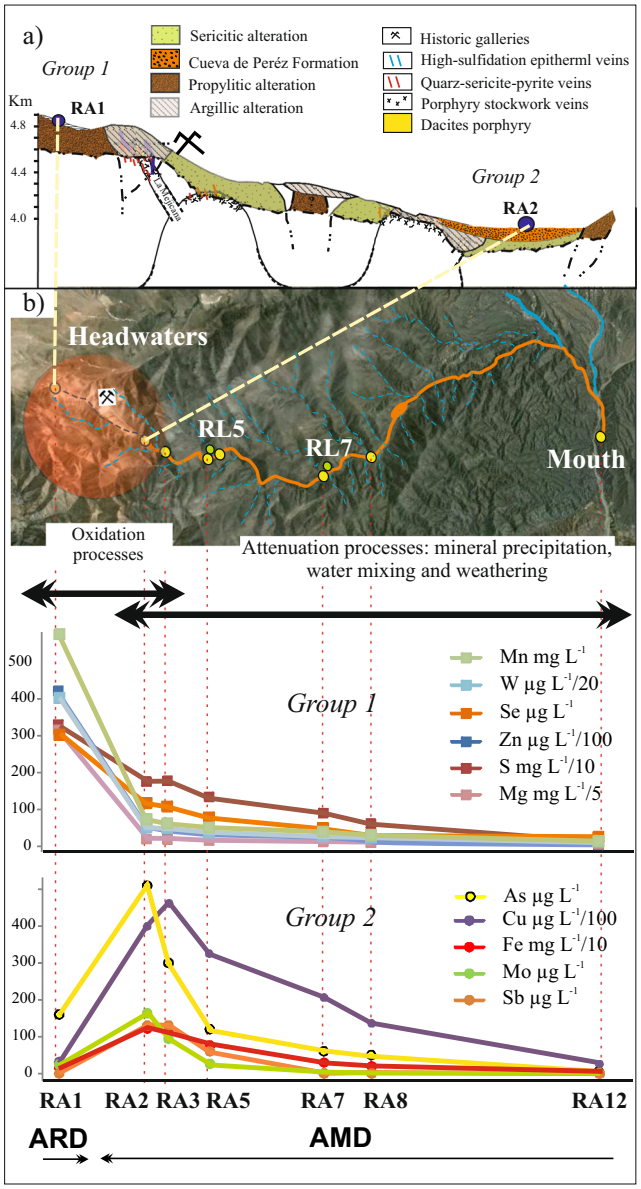

Fig. 4 **a** Blown up profile of Amarillo River uppermost catchment, showing the schematic location of mineral alterations; **b** downstream behavior of dissolved element groups (1 and 2). Concentrations adjusted to fit in the "y" axis. The satellite image shows the most important oxidation and lixiviation area and the subsequent attenuation zone

Mineralogy and geochemistry of solid phases

Different types of non-clastic sediments are recognized along the Amarillo River: efflorescent sulfate salts and ferrous neoformed minerals which may precipitate on the river bed or appear as dark crusts on mineral grains. Field observations showed that efflorescent salts presented bluish-greenish colors in the uppermost catchments, and a whitish appearance downstream, where they became visible less frequently. Precipitated river bed phases corresponded to ferruginous greenish-yellowish precipitates, with soft to spongy consistency and a thickness of ~5 cm. They appeared covering the riverbed or its margins (i.e., the floodplain), with siliciclastic detritus in variable proportions, increasing downstream its relative abundance. Dark crusts corresponded to dark brown gel-like ferruginous precipitates covering not only bed sediments but also some air-exposed pebbles. They were found mainly in the middle and lower basin.

Table 5 summarizes the minerals identified by XRD in the different sediment samples, while XRD diffractogram are included as supplementary information. The mineralogy of

Author's personal copy

Table 5 X-ray diffraction of Amarillo River particulate material

Mineralogy/ sample	Epsonite $MgSO_4$ $7(H_2O)$	Ferro-hexahydrite $MgZnFe(SO_4)_4$ $6(H_2O)$	Halotrichite $FeAl_2$ $(SO_4)_4$ $22(H_2O)$	Mallardite $MnSO_4$ $7(H_2O)$	Melanterite $FeSO_4$ $7(H_2O)$	Pickeringite $MgAl_2(SO_4)_4$ $22(H_2O)$	Jarosite $KFe(SO_4)_2$ $(OH)_6$	Schwertmannite $Fe_{16}O_{16}(SO_4)_3$ $(OH)_{10}$ $10(H_2O)$	Gypsum $CaSO_4$ $2(H_2O)$	K-feldspar $KAlSi_3O_8$	Plagioclase $(Na, Ca)AlSi_3O_8$	Quartz SiO_2
RA1E	X	X										
RA2E			X	X	X	X	X		X	X	X	X
RA5E			X		X	X						
RA2S							X					
RA3S							X			X	X	X
RA5S							X			X	X	X
RAC5S							X	X				X
RA8S							X	X				X
RA12S								X		X	X	X
RA7C							X	X			X	X
RA8C							X	X			X	X

Efflorescent salts are identified as RAnE; bed sediments are identified as RAnS, and dark crusts are identified as RAnC (*n* 1, 2, 3...)

efflorescent salts is represented by sulfates, where Mg–Al phases prevailed over Fe(II). Furthermore, more dehydrated series predominated downstream. Crusts and minerals precipitated on bed sediments were represented by jarosite in the uppermost catchments, whereas schwertmannite was the main sulfate in the middle and lower drainage basin. Detrital minerals (quartz, plagioclase, and K-feldspar) accompanied schwertmannite and jarosite in both, crust and bed, sediments. Maza et al. (2014) interpreted as detrital the jarosite identified when pH > 3 in the middle catchments.

The chemical composition of precipitated phases is shown in Table 6. Efflorescent salts were mainly made up by S, Al, Mg, Mn, and Fe as major elements standing out the amount of Zn, Cu, Co, and Ni, which normally integrate the structure of these sulfates series. Moreover, Ca, Na, and K, as well as Ti and P, appeared as minor components. The geochemical composition of crusts and precipitated minerals showed abundant Fe_2O_3 and S all along the river channel. Iron presented the highest concentration in the upper-middle basin, whereas S showed a relative decrease toward the mouth. Some elements in bed sediments (e.g., As, Cu, Mo, V, Zn, and Cr) reached high concentrations; most of them were associated with S, decreasing their concentrations toward the system's outfall. It is also worthy of mention that lithophile elements (e.g., Ca, Na, Si, Al, Sr) increased their concentrations in the last sample (RA12, lower basin), as it also occurred with Ti, U, Ba, Sc, and Zr, which are common in bed sediments of non-acidic rivers and streams. Downstream, lower concentrations of dissolved elements were coherent with lower metal concentrations in precipitated phases.

Saturation indices

Figure 5a shows some of the SI calculated for the Amarillo River water, by means of a diagram with the precipitation sequence. The mineral phases likely to precipitate were Al-bearing minerals, such as alunite ($KAl_3(SO_4)_2(OH)_6$), basaluminite ($Al_4(OH)_{10}SO_4$), boehmite (AlOOH), diaspore (AlOOH), gibbsite ($Al(OH)_3$), jurbanite ($AlOHSO_4$), and pyrophyllite ($Al_2Si_4O_{10}(OH)_2$); clay minerals, such as beidellite ($(NaKMg_{0.5})_{0.11}Al_{2.33}Si_{3.67}O_{10}(OH)_2$), kaolinite ($Al_2Si_2O_5(OH)_4$), K-mica ($KAl_3Si_3O_{10}(OH)_2$), montmorillonite-Belle Fourche ($(HNaK)_{0.09}Mg_{0.29}Fe_{0.24}Al_{1.57}Si_{3.93}O_{10}(OH)_2$), and montmorillonite-Ca ($Ca_{0.165}Al_{2.33}Si_{3.67}O_{10}(OH)_2$); and Fe-bearing minerals as $Fe(OH)_3$, goethite (FeOOH), hematite (Fe_2O_3), maghemite (Fe_2O_3), magnetite (Fe_3O_4), strengite ($FePO_4{:}2H_2O$); jarosite ($Fe_3(SO_4)_2(OH)_6$) group (jarosite(ss), –K, –Na, and –H); and schwertmannite ($Fe_8O_8(OH)_{5.5}(SO_4)_{1.25}$). Only some representative minerals are included in the figure.

Water in acid drainage systems is commonly supersaturated with respect to a number of iron minerals such as goethite, jarosite, and schwertmannite (e.g., Acero et al., 2006; Asta et al., 2010a; Nordstrom and Alpers, 1999; Sanchez-España

Table 6 Chemical composition of sediments from the study area performed by ICP

ICP Detection limit	S %	CaO	Na_2O	K_2O	MgO	SiO_2	Al_2O_3	Fe_2O_3	MnO	P_2O_5	TiO_2	U mg kg^{-1}	As	Cd	Co	Cu
	0.01	0.01	0.01	0.01	0.01	0.01	0.01	0.01	0.001	0.01	0.001	0.1	1	0.5	0.1	1
RA1E[a]	11.8	0.82	0.60	0.91	9.75	8.47	4.12	2.56	2.15	0.05	0.15	n.d.	n.d.	n.d.	20	199
RA5E[a]	21.4	0.54	0.29	0.99	2.62	5.16	16.02	3.67	4.51	0.06	0.10	n.d.	n.d.	n.d.	56	5381
RA2S	11.3	0.08	0.59	6.55	0.05	1.57	0.45	46.6	0.02	0.25	0.02	<0.1	537	2.8	0.9	466
RA3S	8.86	0.12	0.60	5.87	0.18	13.82	2.86	41.3	0.03	0.32	0.15	1.0	713	1.9	1.8	540
RA8S	6.73	0.11	0.06	0.19	0.24	1.53	1.15	58.9	0.07	0.18	0.02	0.3	372	7.0	7.6	323
RA12S	1.28	1.94	2.13	1.97	0.87	49.57	14.43	15.4	0.08	0.14	0.55	3.5	44	1.2	9.6	310
RA8C[a]	5.60	0.36	0.73	2.47	0.70	18.4	5.57	36.0	0.05	0.22	0.37	n.d.	n.d.	n.d.	122	216

ICP Detection limit	Mo mg kg^{-1}	Ni	Pb	Sb	Sr	V	W	Y	Zn	Ba	Br	Cr	Hf	Rb	Sc	Zr
	2	1	5	0.1	2	5	1	1	1	1	0.5	0.5	0.2	10	0.01	2
RA1E[a]	n.d.	26	56	n.d.	15	n.d.	n.d.	17	12,810	n.d.	n.d.	n.d.	n.d.	42	n.d.	33
RA5E[a]	n.d.	335	n.d.	n.d.	n.d.	n.d.	94	42	14,710	n.d.	n.d.	n.d.	n.d.	39	n.d.	33
RA2S	208	3	13	0.2	98	60	<1	<1	44	32	2.5	10.8	0.3	150	2.42	5
RA3S	320	4	45	5.8	84	87	6	3	79	214	3.4	18.8	2.4	110	5.48	76
RA8S	43	13	12	0.2	2	313	<1	<1	272	2	4.1	31.1	0.2	10	1.16	<2
RA12S	12	15	17	1.1	290	103	2	17	118	434	4.1	49.9	5.3	80	11.4	159
RA8C[a]	36	n.d.	n.d.	n.d.	81	n.d.	n.d.	n.d.	96	290	n.d.	92	n.d.	104	n.d.	142

Different methods have different detection limits; some metals are not detected (n.d.) in efflorescent salts or crusts

[a] Analyses performed by X-ray fluorescence

Author's personal copy

Author's personal copy

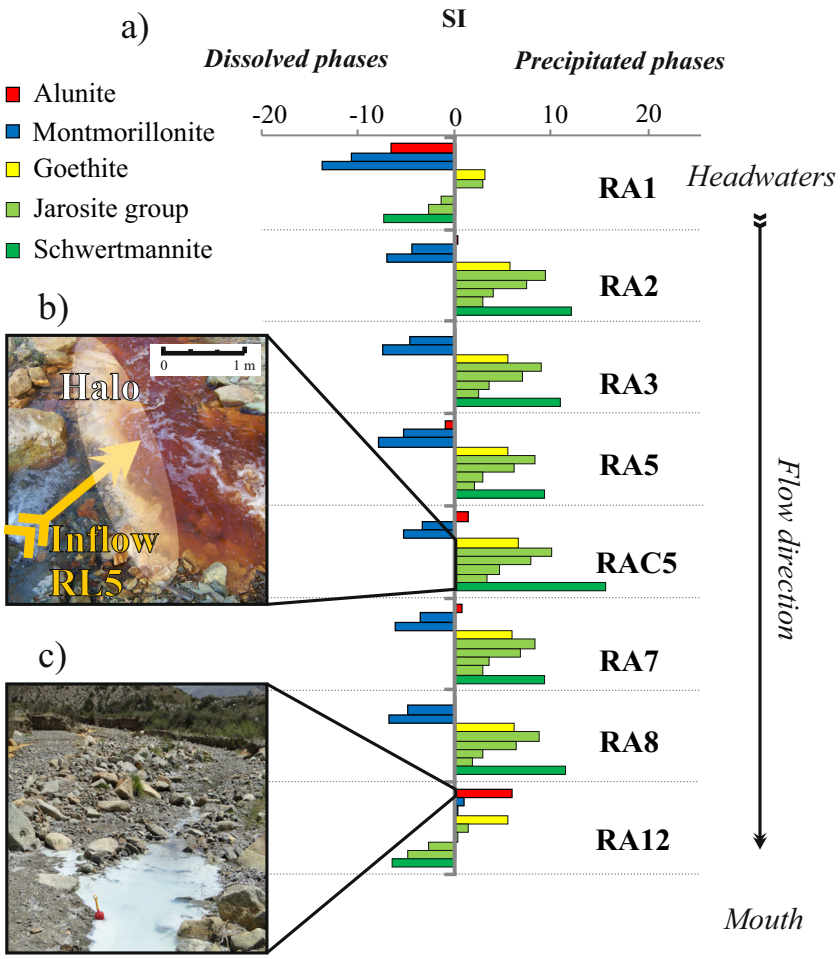

Fig. 5 **a** Mineral SI calculated with PHREEQC for Amarillo River water; **b** halo of Fe-bearing precipitated minerals; **c** Al-bearing precipitated minerals

et al., 2005a, 2005b). Figure 5a shows representative minerals. Many Fe-bearing minerals presented positive SI throughout the drainage basin. In the sample collected downstream the meeting of Amarillo River and a lateral creek (RAC5, middle catchments, Fig. 5b), there were increases in positive SI (e.g., jarosite(Na) from 2.08 to 2.50; schwertmannite from 9.5 to 14). The physicochemical characteristics were re-established a few meters downstream, as evidenced by pH and SI, and field observations (e.g., the noticeable decrease in the amount of iron precipitates).

In the last sample (RA12, downstream the joining of del Marco and Achavil rivers), SI of iron minerals decreased, whereas other minerals exhibited positive SI: alunite (e.g., Fig. 5c) and clay minerals. Al-bearing minerals showed the instability of dissolved Al; when pH reached ~4.5, free Al was no longer stable as a dissolved species and precipitated (Nordstrom, 1982; Bigham and Nordstrom, 2000). The positive SI of montmorillonite does not mean that clays precipitated due to oversaturation, rather they were the product of incongruent dissolution of country rock silicates, mobilized by incoming tributaries. In general, SI values were consistent with the mineralogy identified in the sediment.

Attenuation of dissolved elements

Natural attenuation processes are connected with dissolved concentrations and also with the rate and quantity of neoformed precipitated minerals. The following equation was employed in order to quantify "attenuation" (i.e., geochemical reaction and dilution process which reduce dissolved concentration):

$$A = 100 - \left(\frac{C_i}{C_{imax}} 100\right)$$

A is the relative attenuation, C_i is the concentration of element i, and $C_{i\ max}$ is the maximum concentration of element i. Table 7 shows the relative results for each dissolved element along the basin. Throughout the ~35-km stretch, most metals were almost completely attenuated. There were three sets of elements with dissimilar behavior:

1. Elements which diminished their concentrations >90 % in the first ~9-km stretch (down to RAC5), whose decrease was mainly explained by the formation of jarosite and also of efflorescent salts, which acted as temporary sinks (e.g.,

Author's personal copy

Table 7 Percent attenuation of each dissolved element

	Downstream distance (km) %	W	Y	Zn	Mg	Mn	U	Tl	As	Mo	Ce	S	Fe	Al	Cd	Ni
RA1	0	0	0	0	0	0	33.3	0	68.6	85.3	0	0	87.5	70.8	3.3	52.4
RA2	4.89	89.6	93.2	87.9	94.0	88.8	~100	85.7	0	0	85.4	47.0	0	4.6	0.0	7.1
RA3	5.54	90.1	91.5	89.6	94.2	90.9	0	87.3	41.2	42.3	85.4	46.4	9.0	0	22.1	0.0
RA5	8.83	93.2	93.2	92.4	95.3	92.7	44.4	89.7	76.5	84.0	87.8	59.4	37.6	26.2	43.7	25.6
RAC5	8.84	94.7	94.9	93.8	95.8	94.0	~100	92.1	94.1	92.6	90.2	67.0	55.0	43.1	57.8	41.8
RA7	15.19	95.5	94.9	94.9	96.2	95.0	~100	93.7	88.2	~100	90.2	72.7	75.7	52.8	64.6	50.2
RA8	17.09	96.9	96.6	96.6	97.2	96.6	~100	95.2	90.2	~100	~100	81.3	83.9	67.4	76.0	65.9
RA12	34.37	99.4	96.6	99.3	97.9	99.4	~100	99.2	~100	~100	~100	95.0	100	94.6	95.8	92.9

	Be %	K	Cu	P	Pb	Cr	V	Sb	Te	Co	Se	Si	Sr	Na	Ca
RA1	0.0	99.0	93.3	85.2	71.6	46.4	~100	~100	0	0	0	61.3	0	0	0
RA2	62.5	0.0	13.6	0	10.4	7.1	4.2	0	25.0	15.8	63.3	11.8	78.1	42.5	85.7
RA3	62.5	33.0	0	4.5	0	0	0	0	25.0	11.8	66.7	0.0	82.8	50.4	84.0
RA5	68.8	72.8	29.7	37.7	25.4	28.6	45.8	53.8	50.0	36.4	76.7	18.4	89.1	61.5	86.8
RAC5	78.1	77.0	46.3	51.5	43.3	42.9	75.0	69.2	66.7	52.7	83.3	34.7	89.1	74.4	87.3
RA7	78.1	80.8	55.4	68.1	49.3	53.6	~100	~100	75.0	59.2	86.7	37.6	87.5	78.3	86.7
RA8	87.5	86.2	70.6	78.3	65.7	67.9	~100	~100	83.3	72.1	93.3	52.9	89.1	87.9	88.6
RA12	~100	87.0	94.5	95.5	92.5	~100	~100	~100	83.3	94.6	~100	74.7	67.2	61.6	79.7

"0" means maximum concentration, "~100" means maximum attenuation (≈detection limit)

Author's personal copy

Y, Zn, Mg, Mn, As, and Mo, Table 7). These elements may be released to surface runoff or groundwater during rainfall events (e.g., Hammarstrom, et al. 2005, Romero et al. 2006);

2. Elements which were attenuated all along the basin, mainly related with dilution by groundwater incoming and tributaries, and with neoformed Fe-bearing minerals, such as jarosite or schwertmannite (e.g., S, Cu, Fe, Al, Cd, Ni, Pb, P, Cr, Co). These new phases exhibited small particle size and high surface areas which most likely favored sorption or coprecipitation of significant amounts of trace elements. These processes were particularly noticeable in the lower stretch after joining the tributaries, producing a significant change in the relative attenuation (e.g., Cr from ~68 to ~100 %, Pb from ~66 to ~92 %, Table 7)
3. The last set of elements was probably involved in silicate weathering, which presented a lesser attenuation along the upper and middle basin, and exhibited a variable behavior in the lower reach (e.g., Si, Sr, Na, Ca). This is evidenced of incoming water (i.e., dilution) and the release of cations by silicate weathering. Neither major nor minor or trace elements remained with constant concentration in the solution.

The overall inspection of attenuation dynamics shows that the system modified its physicochemical characteristics as follows: pH increased about 0.05 pH unit per km, while the decrease of electrical conductivity reached about 0.3 mS cm^{-1} km^{-1}. The decrease of dissolved Fe and S was approximately 35 and 90 mg L^{-1} km^{-1}, respectively. However, the attenuation was not proportional to distances between sampling points but varied significantly among them. For example, Fe had a mean decreasing rate of 3500 % km^{-1} between RA5 and RAC5 whereas it reached 3.2 % km^{-1} between RAC5 and RA7. This behavior is due to the influence of tributaries, which not only dilute the Amarillo's main stem but also enhance mineral precipitation. This feature is verifiable for most of the remaining chemical elements.

Geochemical modeling

Modeling results are mere approximations to the system's real behavior, seeking an estimation to the amount of moles transferred between the dissolved and solid phases. The inverse modeling exercise used a known initial solution in order to quantify processes that might have led to the final known solution. To analyze the physicochemical control in the precipitation of newly formed minerals, we compared the inverse modeling simulation in the upper catchments (i.e., from RA3 to RA5) with that corresponding to the Amarillo's middle stretch (i.e., from RA5 to RA8).

Model input files consisted of measured pH, redox potential, temperature, and concentrations of dissolved major ions, metals, and SiO_2 (see Online Resource for additional information). Since surface waters were involved, the equilibrium phase with oxygen was included. The mineral phases chosen for the models were those determined with XRD in sediment samples and some selected minerals which showed positive SI in PHREEQC calculations. Pyrite was included due to the oxidation that occurred in the drainage basin. Some silicates were also included, like those in metamorphic rocks or those which are prone to weathering and produced incongruent products (i.e., clay minerals). Pure water was included in the model to account for evaporation or for the addition of water.

Results (including specific mineral phases) are shown in Table 8. All along the Amarillo River upper stretch, oxidation and hydrolysis released solutes into river water. The precipitation of newly formed minerals was indicated by Fe-bearing sulfates (jarosite) and efflorescent salts (e.g., halotrichite, melanterite).

Models indicate that in the middle drainage basin—besides the dissolution/precipitation of iron sulfates—silicate weathering occurred, with the corresponding clay mineral formation.

From RA3 to RA8, models show that the total sum of dissolved species, which according to the models took part in weathering processes, was of the order of 7 mmol L^{-1}. Dissolved phases were dominated by the weathering of gypsum and of silicates such as K-mica (~2 mmol L^{-1}), favoring the formation of clay minerals (~2 mmol L^{-1}). This stretch

Table 8 Selected PHREEQC inverse models: transferred dissolved and precipitated phases

Model	Phases transferred	Dissolved mmol/Kg H_2O	Precipitated	% Total
Model 3–5	Pyrite	0.01		1.2
	Jarosite-K		0.28	32.4
	Halotrichite		0.20	22.9
	Melanterite		0.35	41.7
	MnHPO4		0.01	1.7
	H2O	11,270		–
Model 5–8				
	Halotrichite		0.71	11.6
	Gypsum	0.30		4.9
	Kmica	2.03		33.1
	Jarosite-K		0.97	15.8
	Jarosite-Na		0.41	6.7
	Illite		1.71	27.9
	H_2O	24,960		–

%Total relative amount transferred for each phase, *Dissolved pure water* water added to the system

Author's personal copy

presents ~3 mmol L^{-1} of newly formed and precipitated mineral phases (efflorescent salts and jarosite). On the other hand, precipitation of Fe-bearing minerals represents ~25 % of the total transferred phases. In contrast, the formation of efflorescent salts reached ~18 % (~1 mmol L^{-1}).

Finally, in a water-mixing exercise performed with PHREEQC, a sample of Amarillo River's middle stretch (RA5) was mixed with an inflowing lateral creek (RL5). The results of this mixing modeling were compared with the actual chemistry of RAC5, which was collected few meters downstream. Input data was 65 % of RA5 and 35 % of RL5. Figure 6 shows the correlation between the modeled sample and RAC5. It shows a significant correlation between both chemical datasets, confirming that modeling the mixing of different waters is a useful tool to predict possible scenarios (e.g., what would happen with the river chemistry when there is an exceptional rainfall or an accidental spillage of polluted water).

Concluding comments

ARD and AMD involve similar geochemical processes. The difference stems from anthropogenic actions which, when occurring, promote and accelerate chemical reactions that characterize AMD. Recent geological history shows that the Amarillo River drainage basin was a typical ARD system, as the sediments accumulated in the paleolake for at least 3500 years (Maza et al. 2014) clearly demonstrates. Mining began in ~1875 and continued until 1925, thus superimposing an AMD scenario on the natural acidic dynamics. A relict of the original ARD is discernible in the uppermost catchments.

Sometimes in these exceptionally acid streams, their extreme acidity is relatively short-lived in the sense that different processes jointly actuate to amend such aggressive characteristic and in relatively short distances, acid attenuation becomes discernible. This is not, however, the case of the Amarillo River, whose pH stays constant throughout a stretch of about 25 km, without the input of an additional acid drainage. This buffering effect is linked to the precipitation of oxy/hydroxy/sulfates and hydroxy/sulfates, which releases protons to the aquatic environment.

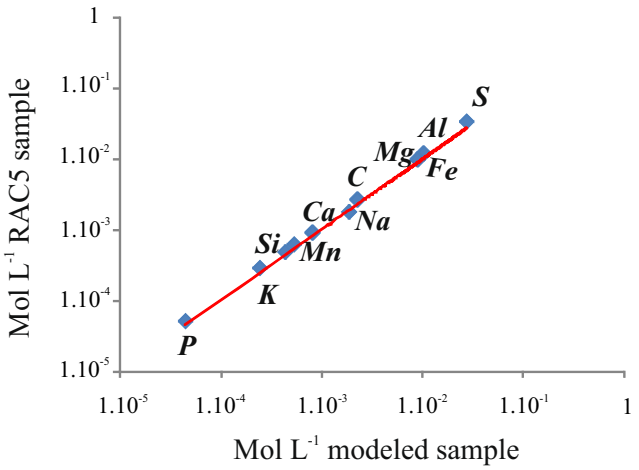

Fig. 6 PHREEQC results of mixing model and its correlation with sample RAC5

Precipitation of solid phases is a direct consequence of the extreme chemistry exhibited by the Amarillo River. In the upper drainage basin (where the mineralized and alteration zones outcrop), the precipitation of jarosite and sulfate-bearing efflorescent salts was evident to the naked eye. PHREEQC modeling showed that in the upper catchments, 0.01 mmol L^{-1} of pyrite reacted through a redox pathway and was transferred to the dissolved phases. In contrast, Fe sulfates would precipitate 0.8 mmol L^{-1} in the upper basin. In the middle stretch, modeling suggested that the supply of solutes was shared by gypsum and k-mica dissolution (~2 mmol L^{-1} for each geochemical process).

The overall result of the processes interacting at the Amarillo River scenario is a significant concentration decrease that follows the flow direction. There are three different mechanisms that appear to control the metal attenuation process. One factor is the precipitation of neoformed minerals. A group of elements (e.g., S, Al, Mg, Fe, K, Mn, Zn, Al, Cd, Ni) contribute to the chemical composition of efflorescent salts, jarosite, and schwertmannite. Furthermore, some heavy metals (e.g., Co, Cu, Cr) coprecipitate by sharing in the crystal structures, whereas As, V, and Mo probably play a relevant role in surface complexation.

Another triggering factor is dilution. It is connected with relatively diluted tributary creeks, groundwater, and atmospheric precipitation, where normally increase pH and lower TDS concentrations. Additionally, the supply of fresh water by tributary creeks favors precipitation due to the ensuing pH increase.

The third intervening factor is lithological: the chemical weathering of country rocks, as the silicate hydrolysis contributes to neutralize acid drainage. In the lowermost basin, weathering appears to reach maximum significance, and major cations (Si, Ca, Sr, and Na) increase their concentrations.

It is clear that investigation of such case studies, particularly through the use of modeling, is a significant aid in finding ways and means to ameliorate environmental problems in mining areas.

Acknowledgments We acknowledge the financial support of the Consejo Nacional de Investigaciones Científicas y Técnicas (CONICET), the Fondo para la Investigación Científica y Tecnológica (FONCYT), both from Argentina. We are also grateful to SECyT (Universidad Nacional de Córdoba) for additional financial support. Our thanks are extended to Ricardo Astini for field assistance. S.M. is a postdoctoral grantee, and K.L.L, G.C., and P.J.D. are members of CICyT, in Argentina's CONICET. We acknowledge the assistance of an anonymous reviewer for important comments and suggestions.

Author's personal copy

References

Acero P, Ayora C, Carrera J (2007) Coupled thermal, hydraulic and geochemical evolution of pyritic tailings in unsaturated column experiments. Geochim Cosmochim Acta 71:5325–5338

Acero P, Ayora C, Torrento C, Nieto JM (2006) The behavior of trace elements during schwertmannite precipitation and subsequent transformation into goethite and jarosite. Geochim Cosmochim Acta 70: 4130–4139

Akcil A, Koldas S (2006) Acid mine drainage (AMD): causes, treatment and case studies. J of Cleaner Prod 14:1139–1145

Asta MP, Ayora C, Román-Ross G, Cama J, Acero P, Gault AG et al (2010a) Natural attenuation of arsenic in the Tinto Santa Rosa acid stream (Iberian Pyritic Belt, SW Spain): the role of iron precipitates. Chem Geol 271:1–12

Asta MP, Ayora C, Acero P, Cama J (2010b) Field rates for natural attenuation of arsenic in Tinto Santa Rosa acid mine drainage (SW Spain). J of Hazardous Materials 177:1102–1111

Asta MP, Cama J, Martínez M, Giménez J (2009) Arsenic removal by goethite and jarosite in acidic conditions and its environmental implications. J of Hazardous Materials 171:965–972

Ball J, Nordstrom DK (1991) User's manual for WATEQ4f with revised thermodynamic database and test cases for calculating speciation of major, trace and redox elements in natural waters. U.S. Geological Survey Water-Resources Investigation Report; 91–183

Bigham JM, Carlson L, Murad E (1994) Schwertmannite, a new iron oxyhydroxysulphate from Pyhasalmi, Finland, and other localities. Mineral Mag 58(393):641–648

Bigham JM, Nordstrom DK (2000) Iron and aluminum hydroxysulphates from acid sulphate waters. Sulphate minerals. Crystallography. Geochem and Environ Significance 40:351–403

Bigham JM, Schwertmann U, Traina SJ, Winland RL, Wolf M (1996) Schwertmannite and the chemical modeling of iron in acid sulfate waters. Geochim Cosmochim Acta 60(12):2111–2121

Blowes DW, Ptacek CJ, Jambor JL, Weisener CG, Paktunc D, Gould WD, Johnson DB (2014) The geochemistry of acid mine drainage (second edition). 131–190, Elsevier Ltd.

Borrego J, López-González N, Carro B, Lozano-Soria O (2005) Geochemistry of rare-earth elements in Holocene sediments of an acidic estuary: environmental markers (Tinto River estuary, southwestern Spain). J of Geochem Exploration 86:119–129

Bowell RJ, Bruce I (1995) Geochemistry of iron ochres and mine waters from Levant mine, Cornwall. Appl Geochem 10:237–250

Brantley SL, Goldhaber MB, Vala Ragnarsdottir K (2007) Crossing disciplines and scales to understand the critical zone 2007. Elements 3: 307–314

Brown JG, Glynn PD (2003) Kinetic dissolution of carbonates and Mn oxides in acidic water: measurement of in situ field rates and reactive transport modeling. Appl Geochem 18:1225–1239

Campbell KM, Gallegos TJ, Landa ER (2015) Biogeochemical aspects of uranium mineralization, mining, milling, and remediation. Appl Geochem 57:206–235

Cánovas CR, Hubbard CG, Olías M, Nieto JM, Black S, Coleman ML (2008) Hydrochemical variations and contaminant load in the Río Tinto (Spain) during flood events. J of Hydrology 350:25–40

Cánovas CR, Olías M, Nieto JM, Sarmiento AM, Cerón JC (2007) Hydrogeochemical characteristics of the Tinto and Odiel rivers (SW Spain). Factors controlling metal contents. Sci Total Environ 2007 373:363–382

Cánovas CR, Olías M, Vazquez-Suñé E, Ayora C, Nieto JM (2012) Influence of releases from a fresh water reservoir on the hydrochemistry of the Tinto River (SW Spain). Sci Total Environ 416:418–428

Caraballo MA, Rimstidt JD, Macías F, Nieto JM, Hochella MF Jr (2013) Metastability, nanocrystallinity and pseudo-solid solution effects on the understanding of schwertmannite solubility. Chem Geol 360-361:22–31

Caraballo MA, Macías F, Rötting TS, Nieto JM, Ayora C (2011) Long term remediation of highly polluted acid mine drainage: a sustainable approach to restore the environmental quality of the Odiel river basin. Environ Poll 159:3613–3619

Caraballo MA, Rötting TS, Macías F, Nieto JM, Ayora C (2009) Field multi-step limestone and MgO passive system to treat acid mine drainage with high metal concentrations. App Geochem 24:2301–2311

Chen CJ, Jiang WT (2012) Influence of waterfall aeration and seasonal temperature variation on the iron and arsenic attenuation rates in an acid mine drainage system. Appl Geochem 27:1966–1978

Cidu R, Caboi R, Fanfani L, Frauet F (1997) Acid drainage from sulfides hosting gold mineralization (Furtei, Sardinia). Environ Geol 30: 231–237

Collo G (2006) Caracterización mineralógica, petrográfica y termobarométrica de las unidades con bajo grado de metamorfismo del Famatina. Ph. D. thesis, Universidad Nacional de Córdoba, Argentina

Delgado J, Pérez-López R, Galván L, Nieto JM, Boskiet T (2012) Enrichment of rare earth elements as environmental tracers of contamination by acid mine drainage in salt marshes: a new perspective. Marine Pollut Bull 64:1799–1808

Fernández-Remolar DC, Prieto-Ballesteros O, Chemtob SM, Morris RV, Ming D, Knoll AK, et al. (2006) Geochemical processes driving the Rio Tinto acidic sedimentation: insights into sedimentary sequences on early Mars. Lunar and Planetary Sci; XXXVII, 1809.pdf

Fernández-Turiel JL, López-Soler A, Llorens JF, Querol X, Aceñolaza P, Durand F et al (1995) Environmental monitoring using surface water, river sediments, and vegetation: a case study in the Famatina range, La Rioja, NW Argentina. Environ Int 21(6):807–820

Fukushi K, Sasaki M, Satoc T, Yanased N, Amanod H, Ikeda H (2003) A natural attenuation of arsenic in drainage from an abandoned arsenic mine dump. Appl Geochem 18:1267–1278

Gandy CJ, Smith JWN, Jarvis AP (2007) Attenuation of mining-derived pollutants in the hyporheic zone: a review. Sci Total Environ 373: 435–446

Giggenbach WF (1997) The origin and evolution of fluids in magmatic-hydrothermal systems. In: Geochemistry of hydrothermal ore deposits. 3d ed, Barnes, ed. Wiley. p. 737–796

Grande JA, de la Torre ML, Cerón JC, Beltrán R, Gómez T (2010) Overall hydrochemical characterization of the Iberian Pyrite Belt. Main acid mine drainage-generating sources (Huelva, SW Spain). J of Hydrology 390:123–130

Hammarstrom JM, Seal RR II, Meier AL, Kornfeld JM (2005) Secondary sulfate minerals associated with acid drainage in the eastern US: recycling of metals and acidity in surficial environments. Chem Geol 215:407–431

Hubbard CG, Black S, Cóleman ML (2009) Aqueous geochemistry and oxygen isotope compositions of acid mine drainage from the Río Tinto, SW Spain, highlight inconsistencies in current models. Chem Geol 265:321–334

Johnson DB, Hallberg KB (2005) Acid mine drainage remediation options: a review. Sci Total Environ 338:3–14

Jönsson J, Persson P, Sjoberg S, Lovren L (2005) Schwertmannite precipitated from acid mine drainage: phase transformation, sulphate release and surface properties. App Geochem 20:179–191

Kawano M, Tomita K (2001) Geochemical modeling of bacterially induced mineralization of schwertmannite and jarosite in sulfuric acid spring water. Am Mineral 86:1156–1165

Kozubal MA, Macur RE, Jay ZJ, Beam JP, Malfatti SA (2012) Microbial iron cycling in acidic geothermal springs of Yellowstone National Park: integrating molecular surveys, geochemical processes, and isolation of novel Fe-active microorganisms. Front Microbiol 3:1–16

Author's personal copy

Lecomte KL, Milana JP, Formica SM, Depetris PJ (2008a) Hydrochemical appraisal of ice- and rock-glacier meltwater in the hyperarid Agua Negra drainage basin. Andes of Argentina Hydrol Proc 22(13):2180–2195

Lecomte KL, García MG, Pasquini AI, Depetris PJ (2008b) Elementos traza disueltos en ríos de montaña: un comportamiento singular XII Reunión Argentina de Sedimentología (XII RAS), Bs As; p: 93

Lecomte KL, Pasquini AI, Depetris PJ (2005) Mineral weathering in a semiarid mountain river: its assessment through PHREEQC inverse modelling. Aquatic Geochem 11(2):173–194

Lei L, Song C, Xie X, Li Y, Wang F (2010) Acid mine drainage and heavy metal contamination in groundwater of metal sulfide mine at arid territory (BS mine, Western Australia). Trans Nonferrous Met Soc China 20:1488–1493

Lindsay MBJ, Moncur MC, Bain JG, Jambor JL, Ptacek CJ, Blowes DW (2015) Geochemical and mineralogical aspects of sulfide mine tailings. Appl Geochem 57:157–177

Losada-Calderon A, McPhail D (1994) The Nevados de Famatina mining district: porphyry- and epithermal-stile mineralization, La Rioja Prov, Argentina 7° Congreso Geológico Chileno Actas volumen II; 1585–9

Lowell JD, Guilbert JM (1970) Lateral and vertical alteration mineralization zoning in porphyry ore deposits. Econ Geol 65:373–408

Macías F, Caraballo MA, Rötting TS, Pérez-López R, Nieto JM, Ayora C (2012) From highly polluted Zn-rich acid mine drainage to non-metallic waters: implementation of a multi-step alkaline passive treatment system to remediate metal pollution. Sci Total Environ 433:323–330

Majzlan J, Navrotsky A, Schwertmann U (2004) Thermodynamics of iron oxides: part III. Enthalpies of formation and stability of ferrihydrite (~Fe(OH)3), schwertmannite (~FeO(OH)3/4(SO4)1/8), and ve-Fe2O3. Geochim. Cosmochim. Acta 68:1049–1059

Maza SN (2010) Caracterización mineralógica y geoquímica de sedimentos lacustres cuaternarios en los Andes Centrales de Argentina Tesis final Master en Geología y Gestión Ambiental de los Recursos Minerales Universidad Internacional de Andalucía y Universidad de Huelva

Maza SN, Collo G, Astini R, Nieto F, Nieto JM (2014) Holocene ochreous lacustrine sediments within the Famatina belt, NW Argentina: a natural case for fossil damming of an acid drainage system. Journal of South American Earth Science 52:149–165

Maza SN (2015) Estudio de unidades asociadas a paleo-drenaje ácido en la región Central de Famatina y su comparación con el actual drenaje ácido de minas. Ph. D. thesis, Universidad Nacional de Córdoba, Argentina, p: 205

Meck ML, Masamba WRL, Atlhopheng J, Ringrose S (2011) Natural attenuation of mining pollutants in the transboundary. Save River Physics and Chemistry of the Earth 36:836–841

Nagorski SA, Moore JN (1999) Arsenic mobilization in the hyporheic zone of a contaminated stream. Water Resour Res 35(11):3441–3450

Nieto JM, Sarmiento AM, Olías M, Canovas CR, Riba I, Kalman J et al (2007) Acid mine drainage pollution in the Tinto and Odiel rivers (Iberian Pyrite Belt, SW Spain) and bioavailability of the transported metals to the Huelva estuary. Environ Int 33:445–455

Nordstrom DK, Blowes DW, Ptacek CJ (2015) Hydrogeochemistry and microbiology of mine drainage. An update Applied Geochemistry 57(2015):3–16

Nordstrom DK, Campbell KM (2014) Modeling low-temperature geochemical ProcessesUS geological survey. Boulder, CO, USA, volume 5:1–38

Nordstrom DK, Alpers CN (1999) Geochemistry of acid mine waters chapter 6, In The Environmental Geochemistry of Mineral Deposits, Reviews in Economic Geology, (eds GS Plumlee and MJ Logsdon) Society of Economic Geologists, Littleton, CO pp; 133–60

Nordstrom DK, Wilde FD (1998) Reduction-oxidation potential (electrode method) In: Field measurements, Vol 9 (A6), US Geological Survey Techniques of Water-Resources Investigations; 20 pp

Nordstrom DK (2011) Mine waters: acidic to circumneutral. ELEMENTS VOL 7:393–398

Nordstrom DK (2009) Acid rock drainage and climate change. J of Geochem Expl 100:97–104

Nordstrom DK (1982) The effect of sulfate on aluminum concentrations in natural waters: some stability relations in the system $A1_2O_3$-SO_3-H_2O at 298 K. Geochim Cosmochim Acta 46:681–692

Olías M, Cánovas CR, Nieto JM, Sarmiento AM (2006) Evaluation of the dissolved contaminant load transported by the Tinto and Odiel rivers (south West Spain). Appl Geochem 21:1733–1749

Olías M, Cerón JC, Fernández I, Moral F, Rodríguez-Ramírez A (2005) State of contamination of the waters in the Guadiamar Valley five years after the Aznalcóllar spill water. Air, and Soil Pollut 166:103–119

Olías M, Nieto JM, Sarmiento AM, Cerón JC, Cánovas CR (2004) Seasonal water quality variations in a river affected by acid mine drainage: the Odiel River (south West Spain). Sci Total Environ 333:267–281

Parkhurst DL, Apello CA (1999) User's guide to PHREEQC (version 2)—a computer code program for speciation, bath-reaction, one-dimensional transport and inverse geochemical calculations United States Geological Survey Water Resource Investigationn Report; 99–4259

Pérez-López R, Delgado J, Nieto JM, Márquez-García B (2010) Rare earth element geochemistry of sulphide weathering in the São Domingos mine area (Iberian Pyrite Belt): a proxy for fluid–rock interaction and ancient mining pollution. Chem Geol 276:29–40

Pérez-López R, Nieto JM, López-Cascajosa MJ, Díaz-Blanco JM, Sarmiento AM, Oliveira V, Sánchez-Rodas D (2011) Evaluation of heavy metals and arsenic speciation discharged by the industrial activity on the Tinto-Odiel estuary. SW Spain Marine Pollut Bull 62:405–411

Pudack C, Halter E, Heinrich A, Pettke T (2009) Evolution of magmatic vapor to gold-rich epithermal liquid: the porphyry to epithermal transition at Nevados de Famatina. Northwest Argentina Bul of the Soc of Ec Geological 104:449–477

Romero A, Gonzáles I, Galán E (2006) The role of efflorescent sulfates in the storage of trace elements in stream waters polluted by acid mine-drainage: the case of Peña del Hierro. Southwestern Spain The Canadian Mineral 44:1431–1446

Sanchez-España J, López Pamo E, Santofimia Pastor E, Reyes Andrés J, Martín Rubı JA (2005a) The natural attenuation of two acidic effluents in Tharsis and La Zarza-Perrunal mines (Iberian Pyrite Belt, Huelva, Spain). Environ Geol 49:253–266

Sanchez-España J, López Pamo E, Santofimia Pastor E, Anduvire O, Reyes Andrés J, Barettino D (2005b) Acid mine drainage in the Iberian Pyrite Belt (Odiel river watershed, Huelva, SW Spain): geochemistry, mineralogy and environmental implications. Appl Geochem 20:1320–1356

Sarmiento AM, DelValls A, Nieto JM, Salamanca MJ, Caraballo MA (2011) Toxicity and potential risk assessment of a river polluted by acid mine drainage in the Iberian Pyrite Belt (SW Spain). Sci Total Environ 409:4763–4771

Sarmiento AM, Olías M, Nieto JM, Cánovas CR, Delgado J (2009) Natural attenuation processes in two water reservoirs receiving acid mine drainage. Sci Total Environ 407:2051–2062

Stumm W, Sulzberger B (1992) The cycling of iron in natural environments: considerations based on laboratory studies of heterogeneous redox processes. Geochim et Cosmochim Acta 56:3233–3257

Torres CA, Gianni R, Salvioli G, Ferrés CA (2007) Estudio hidrogeológico preliminar de la cuenca subterránea adyacente al faldeo oriental del norte de la Sierra de Famatina. Informe

Author's personal copy

Técnico, IT-255. Administración Provincial del Agua – Instituto Nacional del Agua, Acta complementaria N° 19, p

Urbieta MS, González Toril E, Giaveno MA, Aguilera Bazán A, Donati ER (2014) Archaeal and bacterial diversity in five different hydrothermal ponds in the Copahue region in Argentina. Syst Appl Microbiol 37:429–441

Wunderlin C, Maza SN, Collo G, DoCampo M, Nieto F (2014) Caracterización de minerales de arcilla en depósitos asociados a drenaje ácido de roca de la Fm. Corral Amarillo, Famatina. Actas XIX Congreso Geológico Argentino 2014. Córdoba, Argentina

Younger PL (1997) The longevity of minewater pollution: a basis for decision-making. The Sci Total Environ 194:457–466

Yu JY, Heo B, Choi IK, Cho JP, Chang HW (1999) Apparent solubilities of schwertmannite and ferrihydrite in natural streamwaters polluted by mine drainage. Geochim Cosmochim Acta 63:3407–3416